Island Arc

WILEY

Island Arc

RESEARCH ARTICLE

Origin of Silicic Magmas at Kibblewhite Volcano: Implications for Bimodal Volcanism in the Kermadec Arc

Yasuhiro Hirai[1,2] | Yoshihiko Tamura[2]

[1]Division of Natural System, Kanazawa University, Kanazawa, Ishikawa, Japan | [2]Research Institute for Marine Geodynamics, Japan Agency for Marine-Earth Science and Technology (JAMSTEC), Yokosuka, Kanagawa, Japan

Correspondence: Yasuhiro Hirai (deep.forest.alliance@gmail.com)

Received: 18 August 2025 | **Revised:** 8 March 2026 | **Accepted:** 16 March 2026

Keywords: bimodal volcanism | fractional crystallization | parallel differentiation | primary magma

ABSTRACT

This study investigates the origin of silicic magmas at the Kibblewhite Volcano in the Kermadec arc. Two alternative differentiation pathways are evaluated: fractional crystallization of primary basaltic magmas producing low-Mg andesites, and fractional crystallization of primary andesitic magmas represented by magnesian andesites. Major- and trace-element geochemistry, rare earth element (REE) systematics, geothermobarometric constraints, and thermodynamic modeling demonstrate that the low-Mg andesites represent already evolved melts and cannot generate the observed dacitic to rhyolitic magmas through further crystallization. In contrast, magnesian andesites show close agreement with the silicic magmas in both major-element and REE compositions, indicating that they provide a viable parental magma for the silicic magmas at Kibblewhite Volcano. These results indicate that two distinct differentiation pathways coexist beneath the Kibblewhite Volcano, in which basaltic and andesitic primary magmas evolve independently to produce low-Mg andesites and dacitic to rhyolitic magmas, respectively. When considered in a broader context, parallel differentiation of basaltic and andesitic primary magmas may also contribute to the bimodal SiO_2 distributions characteristic of the Kermadec Arc; however, this arc-scale application should be regarded as a working hypothesis requiring further evaluation at other volcanic centers.

1 | Introduction

Submarine volcanoes frequently produce explosive eruptions that significantly impact Earth's surface. For instance, the 2012 Havre Volcano eruption in the Tonga arc (Carey et al. 2014; Jutzeler et al. 2014; Velasquez et al. 2018) and the 2021 Fukutoku-Oka-no-Ba eruption in the Ogasawara arc (Yoshida et al. 2022, 2023) created extensive pumice rafts, disrupting the ecology and economy of the Western Pacific. Similarly, the 2022 Hunga Tonga-Hunga Ha'apai eruption generated tsunamis observed worldwide (Lynett et al. 2022). These events underscore the importance of understanding the origin of magmas in oceanic arcs for both geological research and disaster mitigation.

The Kermadec arc, an active oceanic arc in the Southwestern Pacific, is characterized by a thin crust (< 15 km) (Bassett et al. 2016) and bimodal volcanism involving basaltic (50–57 wt.% SiO_2) and rhyolitic (63–73 wt.% SiO_2) magmas (Smith, Worthington, et al. 2003; Wright et al. 2006). While the origin of silicic magmas in the Kermadec arc has been debated, consensus suggests that they are derived from basaltic sources. Early studies (Smith et al. 2010; Smith, Stewart, and Price 2003; Smith, Worthington, et al. 2003; Smith and Price 2006) proposed that lower crustal amphibolite melting could generate silicic magmas; however, recent research favors a model where 70%–80% fractional crystallization of basaltic melt produces dacitic to rhyolitic magmas (Barker et al. 2013;

Haase et al. 2006; Keith et al. 2018; Knafelc et al. 2020). This preference arises because (1) the oxygen isotope compositions of dacites and rhyolites more closely match mantle-derived melts (Barker et al. 2013; Haase et al. 2011), (2) mafic blebs are observed in the dacites and rhyolites (Barker et al. 2013), and (3) amphibolite melting does not adequately explain the rare earth element (REE) concentrations in silicic magmas (Barker et al. 2013; Brophy 2008).

Recently, a study by Hirai et al. (2023) identified magnesian andesites at the Kibblewhite Volcano and estimated their primary melt compositions, referred to as Kibblewhite high-magnesian andesites (HMAs). These melts are interpreted as mantle-derived andesitic magmas generated under relatively shallow upper-mantle conditions (~1–1.3 GPa), rather than at pressures characteristic of deeper mantle melting. Additionally, Hirai et al. (2024) reported olivine-hosted primitive basaltic melt inclusions (PBMIs) from the same volcano, representing deeper mantle-derived magmas predating the magnesian andesites. These findings suggest that the thin crust of the Kermadec arc facilitates the coexistence of both basaltic and andesitic primary magmas, even within a single volcanic system. Consequently, focusing solely on basaltic sources may be insufficient when explaining the origin of rhyolitic magmas in this arc.

Accordingly, the primary objective of this study is to constrain the origin of silicic magmas at the Kibblewhite Volcano through integrated geochemical, geothermobarometric, and thermodynamic approaches. We focus on evaluating whether the silicic magmas can be derived from fractional crystallization of basaltic primary magmas or whether differentiation of primary andesitic magmas provides a more consistent explanation. Based on the results obtained at Kibblewhite, we further explore the implications of coexistence of two differentiation pathways for understanding bimodal magmatism in the Kermadec arc. This arc-scale discussion is presented as a working hypothesis, intended to provide a conceptual framework for future studies, rather than to propose a universal model applicable to all Kermadec volcanoes. Importantly, this study does not seek to dismiss established models invoking extensive fractional crystallization of basaltic magmas, but instead aims to clarify the conditions under which andesitic parental magmas may contribute to the generation of silicic melts.

2 | Geological Background

2.1 | Kibblewhite Volcanic System

The Kermadec arc is an intra-oceanic island arc extending from northeast of the North Island of New Zealand to the Tonga arc, formed by subduction of the Pacific Plate beneath the Australian Plate. Kibblewhite Volcano is a submarine volcanic system located in the southern part of the Kermadec arc and consists of a main edifice centered at approximately 34.6° S, 179.2° E, together with several satellite cones (KI1–KI4; Figure 1). Volcanic rocks have been recovered from these edifices by dredging during multiple expeditions (Wright et al. 2006; Hirai et al. 2023; Figure 1). The recovered lavas span a wide compositional range from basalt to rhyolite

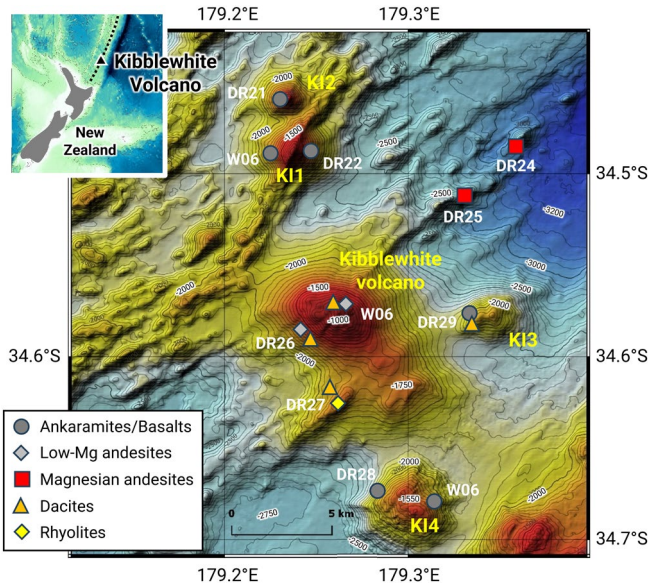

FIGURE 1 | Bathymetric map of the Kibblewhite Volcano and the sample location. The original image is after Hirai et al. (2023).

(Figure 2). Based on petrographic observations and geochemical characteristics, Hirai et al. (2023) classified these rocks into several magma types, and the same classification is adopted in this study. The petrographic characteristics of each magma type are summarized below.

2.1.1 | Ankaramites and Basalts

Ankaramites and basalts were collected from the satellite cones KI1–KI4 and not from the main edifice of the Kibblewhite Volcano (Figure 1). Among samples with basaltic whole-rock compositions, those containing more than 30 vol.% olivine + clinopyroxene are classified as ankaramites, whereas the remainder are referred to as basalts. Ankaramites are also distinguished from basalts by their whole-rock compositions, characterized by MgO contents exceeding 10 wt.%. Ankaramites are crystal-rich but either highly vesicular (Figure S1a) or characterized by concentric degassing cracks radiating from their interiors (Figure S1b), indicating eruption onto the seafloor as lava flows or volcanic bombs. Olivine and clinopyroxene phenocrysts commonly reach up to ~5 mm in size (Figure S1c), whereas plagioclase is restricted to the groundmass and is typically < 1 mm (Figure S1d). The coarse-grained olivine and clinopyroxene phenocrysts are highly magnesian, with compositions comparable to mantle peridotite, and minerals are unzoned or normally zoned from core to rim (Figure S1e).

In contrast, basalts are aphyric to moderately phyric, with total phenocryst contents generally < 20 vol.%, and display moderate vesicularity (Figure S2a,b). Phenocrysts consist of olivine + plagioclase ± clinopyroxene and commonly form glomerophyric aggregates (Figure S2c,d). Olivine and clinopyroxene phenocrysts are mostly < 1 mm in size, whereas plagioclase phenocrysts occasionally exceed 2 mm. These minerals are unzoned or normally zoned, with larger plagioclase phenocrysts locally showing pronounced normal zoning from core to rim (Figure S2e).

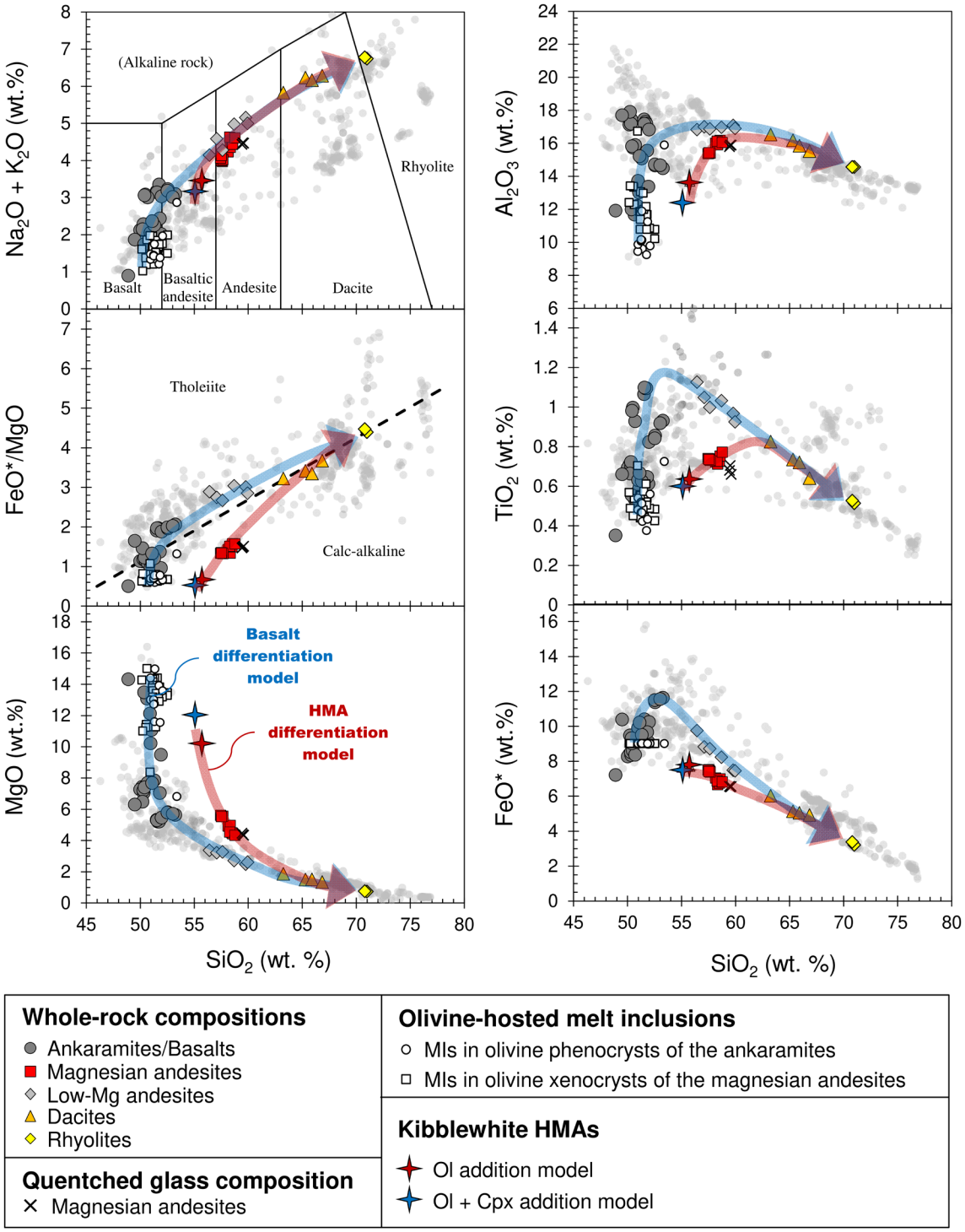

FIGURE 2 | Major element variations in volcanic rocks from the Kibblewhite Volcano. Differentiation trends for primary andesites (Kibblewhite HMAs) and basalts (primitive basaltic melt inclusions: PBMIs) are illustrated with red and blue arrows, respectively. Data points represent volcanic rocks and glasses from Kibblewhite Volcano (Hirai et al. 2023), while gray circles indicate published data from the Kermadec arc (Gamble, Smith, et al. 1993, 1993, 1996, 1997; Ewart et al. 1994; Turner et al. 1997; Haase et al. 2002, 2006; Wright et al. 2006; Wysoczanski et al. 2012; Barker et al. 2013; Timm et al. 2014, 2016). Open squares and circles show olivine-hosted melt inclusions from magnesian andesites and ankaramites (Hirai et al. 2024). The discrimination boundary line in the FeO*/MgO-SiO_2 diagram follows Miyashiro (Miyashiro 1974).

2.1.2 | Magnesian Andesites

Magnesian andesites were collected from a NE–SW-trending ridge located on the northeastern flank of the Kibblewhite Volcano (Figure 1). In this study, the term magnesian andesite refers exclusively to samples recovered at site DR25. These lavas lack manganese coatings on their surfaces and contain fresh quenched glass (Figure S3a). They are aphyric and highly vesicular (Figure S3b) and consist of olivine and clinopyroxene microphenocrysts (<0.4 mm), with plagioclase absent even from the

groundmass (Figure S3c,d). Rare olivine xenocrysts (>0.5 mm; Fo = 90–92) are mantled by thin rims with compositions similar to those of the microphenocrysts (Fo≈85; Figure S3e). The quenched glass contains a minor amount of acicular quench crystals (Figure S3f) but has a composition indistinguishable from the whole-rock chemistry (Figure 2). Olivine and clinopyroxene microphenocrysts show similar Mg# values (Mg#≈85) and lack pronounced zoning (Figure S3g). The Fo contents of olivine in equilibrium with the whole-rock compositions are consistent with those of the olivine microphenocrysts (Hirai et al. 2023). Based on these features, Hirai et al. (2023) concluded that the DR25 magnesian andesites were not produced by disequilibrium processes such as magma mixing or crustal assimilation.

In contrast, magnesian andesites from site DR24 commonly contain reversely zoned pyroxenes (Hirai et al. 2023), suggesting magma mixing between DR25-type magnesian andesite and more evolved magmas such as dacite or rhyolite.

2.1.3 | Low-Mg Andesites

Low-Mg andesites were collected from areas surrounding the main edifice of the Kibblewhite Volcano (Figure 1). They are microphyric rocks composed of clinopyroxene + orthopyroxene + plagioclase + magnetite and display low vesicularity. The groundmass contains little glass and is largely filled by fine-grained acicular crystals (Figure S4a,b). The most evolved sample (DR26-1) contains ilmenite (Figure S4c). Clinopyroxene, orthopyroxene, and plagioclase commonly form glomerophyric aggregates (Figure S4d). These minerals are generally unzoned or show normal zoning (Figure S4e).

2.1.4 | Dacites and Rhyolites

Dacites and rhyolites were collected from the vicinity of the main edifice of the Kibblewhite Volcano (Figure 1). Dacites are pumiceous rocks composed of clinopyroxene + orthopyroxene + plagioclase ± amphibole phenocrysts set in a vesicular, glassy groundmass (Figure S5a,b). Phenocrysts locally reach ~1 mm in size, and magnetite and ilmenite also crystallize in the groundmass (Figure S5c). Clinopyroxene + orthopyroxene + plagioclase form glomerophyric aggregates (Figure S5d). Most minerals are unzoned or normally zoned, although weak reverse zoning is locally observed (Figure S5e). Rhyolites are similarly pumiceous but are dominated by amphibole + orthopyroxene + plagioclase phenocrysts in a vesicular glassy groundmass, with clinopyroxene being rare or absent (Figure S6a,b). Minerals are mostly unzoned or normally zoned (Figure S6c), and mafic minerals generally exhibit lower Mg# values than those in dacites.

2.2 | Primary Magmas at Kibblewhite Volcano

2.2.1 | Andesitic Primary Magma

Hirai et al. (2023) argued that the magnesian andesites are not products of magma mixing or other disequilibrium processes, despite containing minor olivine xenocrysts, because the lavas are aphyric and olivine and clinopyroxene microphenocrysts are in equilibrium with the compositions of the quenched glass. On this basis, they inferred that the primary magma composition could be reconstructed by reversing crystal fractionation. Primary andesitic magma compositions were estimated by incrementally adding olivine to the magnesian andesite compositions until the Ni contents of olivine in equilibrium with the melt reached values comparable to mantle olivine (~0.4 wt.% NiO; olivine-addition model). An alternative model simultaneously added olivine and a realistic maximum amount of clinopyroxene (6%) to account for clinopyroxene fractionation (olivine + clinopyroxene addition model). Both approaches yield similar primary magma compositions converging on SiO_2 contents of ~55 wt.% (Figure 2), requiring 12% olivine addition in the former model and 15% olivine + 6% clinopyroxene in the latter. These compositions are consistent with high-magnesian andesites reported from other island arcs, and were termed "Kibblewhite HMAs" (Hirai et al. 2023). Based on their trace element and isotopic similarities to coexisting basalts and the thin crust of the Kermadec arc, Hirai et al. (2023) concluded that the Kibblewhite HMAs could be generated by hydrous melting of the shallow mantle wedge beneath the Kibblewhite Volcano, at conditions of approximately 1.1–1.3 GPa with 3.2–5.5 wt.% H_2O.

2.2.2 | Basaltic Primary Magma

Hirai et al. (2024) investigated partially crystallized melt inclusions hosted in olivine xenocrysts within magnesian andesites and in olivine phenocrysts from ankaramites. These melt inclusions were homogenized using a heating stage and analyzed to recover their original melt compositions. Most inclusions are hosted in high-Fo olivine (Fo ≥ 90), and the reconstructed melt compositions closely match the whole-rock compositions of ankaramites (Figure 2). In particular, the trace element compositions of melt inclusions in ankaramites are indistinguishable from those of their host rocks (e.g., DR28-25), indicating that ankaramites are not olivine–clinopyroxene cumulates but represent one of the basaltic primary magmas of the Kibblewhite volcanic system. In contrast, melt inclusions in olivine xenocrysts from magnesian andesites display trace element compositions distinct from their host lavas, suggesting that these xenocrysts were derived from earlier ankaramitic magmas predating magnesian andesite activity. From the compositional diversity of the melt inclusions, Hirai et al. (2024) concluded that ankaramites formed when basaltic primary melts produced by mantle peridotite melting reacted with low-pressure lithospheric mantle during ascent, dissolving clinopyroxene. Assuming ~3 wt.% H_2O in the pre-reaction basaltic primary melt, they estimated generation conditions of ~1310°C and ~1.6 GPa. These results imply that ankaramites and Kibblewhite HMAs were generated at different depths and under distinct melting conditions within the mantle beneath the Kibblewhite Volcano.

2.3 | Potential Magma Differentiation Pathways at Kibblewhite Volcano

At Kibblewhite Volcano, two types of primary magmas—basaltic and andesitic—are inferred to form at different depths

beneath the volcanic system. In addition to these primitive magmas, silicic magmas ranging from dacite to rhyolite are also erupted. Previous studies have primarily considered genetic links between silicic magmas and basaltic parents; however, the occurrence of a primary andesitic magma at the Kibblewhite Volcano requires that potential relationships between andesitic and silicic magmas also be evaluated.

Accordingly, two magma differentiation pathways are considered in this study. In the basalt differentiation model, primary basaltic magma evolves into low-Mg andesite and subsequently generates dacitic and rhyolitic magmas (blue arrows in Figure 2). In contrast, the HMA differentiation model involves the evolution of primary andesitic magma into magnesian andesite, followed by the generation of dacitic and rhyolitic magmas (red arrows in Figure 2). Both low-Mg and magnesian andesites exhibit Sr–Nd–Hf–Pb isotopic compositions consistent with those of the dacites and rhyolites (Figure S7), indicating that either pathway could, in principle, produce the observed silicic magmas. In this study, we estimate the pressure–temperature conditions of each magma type and apply fractional crystallization modeling to evaluate which of these two differentiation pathways more plausibly accounts for the origin of the dacitic and rhyolitic magmas at the Kibblewhite Volcano.

3 | Methods

3.1 | Geothermobarometry

The chemical compositions of mineral phases in volcanic rocks from the Kibblewhite Volcano were reported as the supplementary data in Hirai et al. (2023), enabling us to estimate the magmatic conditions of these magmas. Based on the observed mineralogy, pre-eruptive magmatic temperature, water content, pressure, and oxygen fugacity were determined using the following geothermobarometers. These geothermobarometers were applied to euhedral minerals that do not exhibit reverse zoning. Where calculations required the use of two or more mineral phases, analyses were restricted to minerals forming glomerocrysts or occurring in close spatial proximity, in order to maximize the likelihood of equilibrium. Because whole-rock compositions are treated as proxies for melt compositions in this study, mineral core compositions were preferentially used to minimize the influence of late-stage eruptive processes such as degassing and rapid decompression. The estimated magmatic conditions are summarized in Table S1.

3.1.1 | Temperatures

We used the following geothermometers depending on the mineral phases in the samples: (1) olivine-melt geothermometer (Sugawara 2000); calculated temperatures were only employed when the Fe/Mg exchange partition coefficient (K_D) was in the range of 0.3 ± 0.03, (2) clinopyroxene geothermometer (Wang et al. 2021) for only basaltic and andesitic samples, (3) paired clinopyroxene-orthopyroxene geothermometer (K. D. Putirka 2008); calculated temperatures were only employed where the Fe/Mg ratio was in the equilibrium range ($K_D = 1.09 \pm 0.14$), (4) coexisting ilmenite-magnetite geothermometer (Lepage 2003), and (5) amphibole thermometer (K. Putirka 2016).

3.1.2 | Water Contents

Olivine-melt geothermometer (Sugawara 2000) and the clinopyroxene geothermometer (Wang et al. 2021), which are dependent on H_2O content of the melt, were integrated with a plagioclase-melt hygrometer (Waters and Lange 2015) to simultaneously estimate temperature and water content. In this method, the final temperature and water content were determined by repeating iterative calculations in which the results obtained from the geothermometers and the hygrometer were substituted into each other. For amphibole-bearing samples, water contents were further refined using an amphibole hygrometer (Ridolfi and Renzulli 2012).

3.1.3 | Pressures

Pressure conditions were obtained using clinopyroxene barometer (Wang et al. 2021) for basaltic and andesitic samples and amphibole barometer (Ridolfi 2021) for amphibole-bearing samples. For the amphibole barometer, we employed only the results that were validated as "Overall OK" in the spreadsheet of Ridolfi (2021).

3.1.4 | Oxygen Fugacity

Oxygen fugacity (fO_2) was calculated using a solution model for coexisting magnetite and ilmenite (Spencer and Lindsley 1981) and magnetite-melt oxybarometers (Arató and Audétat 2017).

3.2 | Least-Square Mass Balance Calculation

The basalt and HMA differentiation models were evaluated using least-squares mass balance calculations based on the actual compositions of melt and phenocryst phases (Table S2). The calculations were conducted using OPTIMASBA Microsoft Excel spreadsheet (Cabero et al. 2012) with chemical compositions for parent magmas, daughter magmas, and fractionated phases derived from literature data (Hirai et al. 2023). The fraction of residual melt, along with the mineral assemblages and their proportions among the fractionated minerals, is summarized in Table S3. The calculation of REE concentration in the modeled daughter magmas was performed using the proportions of fractionating phenocryst phases and crystal–liquid partition coefficients, in accordance with the Rayleigh fractionation model. Partition coefficients for REEs were taken from Ewart et al. (1994) for olivine, clinopyroxene, and orthopyroxene; Bédard (2006) for plagioclase; Nandedkar et al. (2016) for amphibole; and Nielsen et al. (1992) for magnetite.

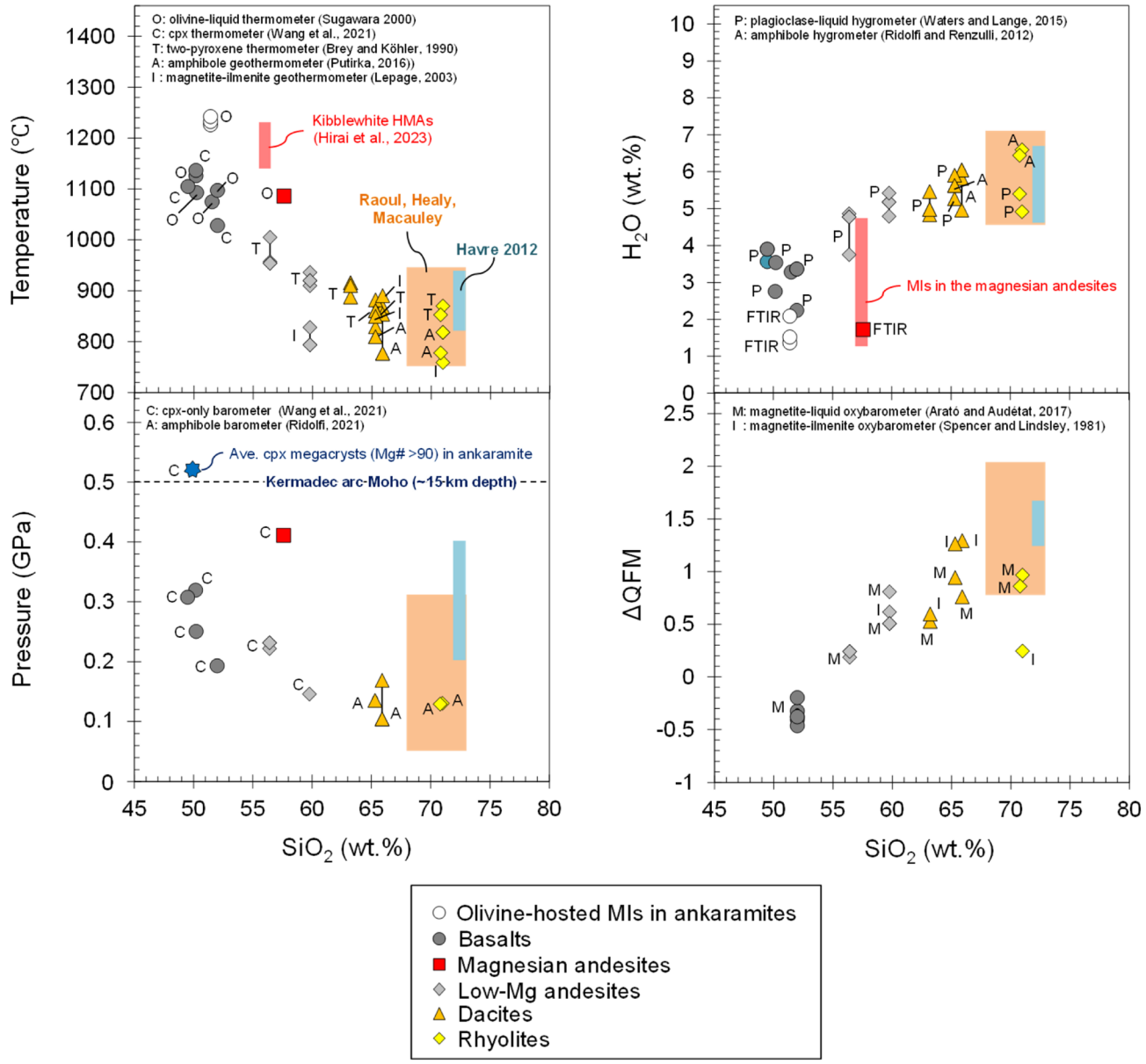

FIGURE 3 | Calculated magmatic conditions (temperature, water content, pressure, and oxygen fugacity) for Kibblewhite magmas based on geothermobarometric analyses. The red shaded area highlights the estimated conditions for Kibblewhite HMAs (Hirai et al. 2023) while the orange and purple regions represent conditions for rhyolitic pumices from Raoul, Healy and Macauley (Barker et al. 2013) and the 2012 Havre Volcano eruption (Knafelc et al. 2020), respectively. The alphabetic labels near the data points denote the geothermobarometers used to determine these values (refer to the references within the graph).

3.3 | Thermodynamic Modeling

Thermodynamic fractional crystallization calculations were performed using Rhyolite-MELTS ver. 1.2 (Ghiorso and Gualda 2015) and COMAGMAT ver. 3.75 (Ariskin and Barmina 2004). The initial melt compositions, cited from the Kibblewhite HMAs and PBMIs, are summarized in Table S4. Given the broad range of CaO/Al_2O_3 ratios observed in PBMIs (Hirai et al. 2024), two representative compositions with ratios of 0.85 and 1.11 were selected for modeling. The initial melts were assumed to contain 1.0 wt.% and 3.0 wt.% H_2O and were crystallized under isobaric conditions at pressures of 3.0 kbar and 5.0 kbar, with oxidation states set to QFM and ΔQFM +1. These conditions were assumed based on the geothermobarometric estimation.

4 | Results

4.1 | Magmatic Conditions

Figure 3 presents the estimated magmatic conditions (temperature, water content, pressure, and oxygen fugacity) derived from multiple geothermobarometers. The geothermometers indicate that magnesian andesites display temperatures comparable to basalts (~1100°C), whereas low-Mg andesites exhibit

similar or slightly higher temperatures to dacites and rhyolites (800°C–1000°C). Geohygrometers estimate water contents of 2–4 wt.% for basalts and 4–7 wt.% H_2O for low-Mg andesites, dacites, and rhyolites. Geobarometers distinguish pressure conditions between basalts (~0.2–0.3 GPa) and magnesian andesites (~0. GPa). Low-Mg andesites exhibit pressure estimates (~0.1–0.2 GPa) that are comparable to those of dacites and rhyolites. The average core composition of clinopyroxene megacrysts (Mg# > 90) in the ankaramite (sample DR28-25) yields a pressure estimate of ~0.52 GPa, corresponding to pressures near the Moho depth of the Kermadec arc (~15 km). Oxybarometers estimate oxygen fugacity values for low-Mg andesites (QFM +0.1 to QFM +0.8), which overlap with those of dacites and rhyolites (QFM +0.5 to QFM +1.3). These magmatic conditions for rhyolites align with those of other rhyolites in the Kermadec arc, such as those from Raoul, Healy, and Macauley (Barker et al. 2013), and the 2012 Havre Volcano eruption (Knafelc et al. 2020). These estimates suggest that the magnesian andesites have high-temperature and high-pressure conditions akin to basalts, distinctly differing from low-Mg andesites while geohygrometers and oxybarometers are not directly applicable to magnesian andesites.

4.2 | Mass Balance Model

The mass balance calculations indicate that both the HMA and basalt differentiation models successfully reproduce the major element compositions of dacites and rhyolites with a low residual sum of squares (Table S2). To further evaluate the parent-daughter relationships, we calculated the REE concentrations of the modeled daughters. Figure 3 shows the REE concentrations for the low-Mg andesite–dacite, magnesian andesite–dacite, and dacite–rhyolite intervals. The results revealed that the major elements of dacite could be reproduced after ~44% fractional crystallization of low-Mg andesite, but its REE concentrations did not match (Figure 4A). In contrast, both the major and REE compositions of dacite were accurately reproduced after ~39% fractional crystallization of magnesian andesites (Figure 4B), while the major and REE compositions of rhyolite were reproduced after ~25% fractional crystallization of dacites (Figure 4C). These findings suggest that dacites and rhyolites are more plausibly formed by fractional crystallization of magnesian andesites rather than low-Mg andesites, particularly in terms of REE concentrations.

Moreover, least-squares mass-balance calculations demonstrated that the primary andesite differentiation model is significantly more efficient in generating silicic magmas than the basalt differentiation model. The HMA differentiation model yielded 46% rhyolitic melts, whereas the basalt differentiation model required more extensive crystal fractionation, producing only 13% rhyolitic melt (Table S3).

4.3 | Thermodynamic Model

Thermodynamic fractional crystallization calculations were conducted using initial compositions derived from the Kibblewhite HMAs and PBMIs. Figure 5 illustrates the representative compositional evolution of the calculated liquids

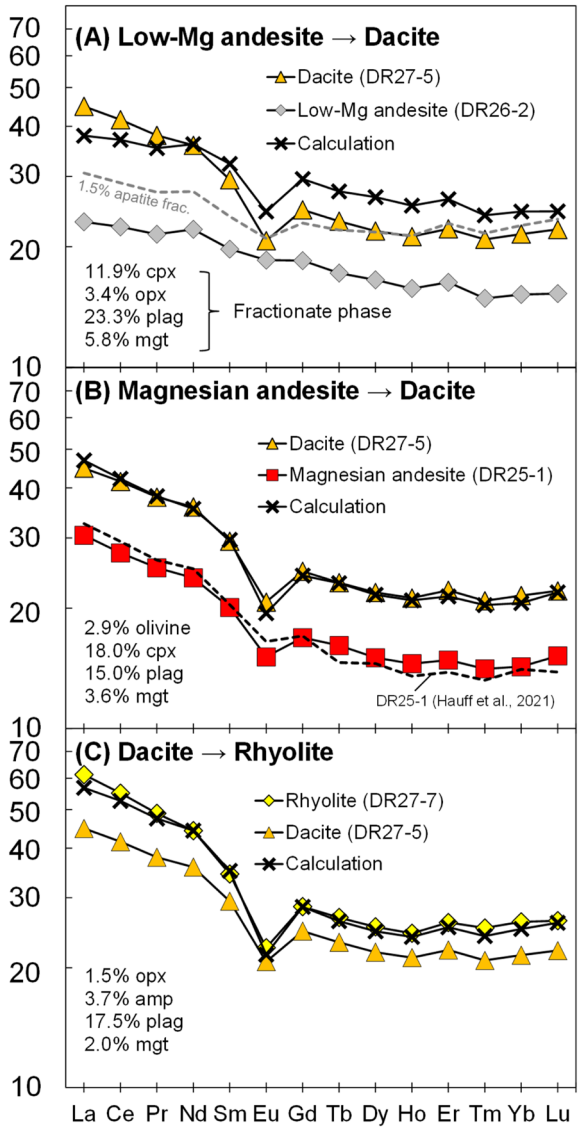

FIGURE 4 | Chondrite-normalized rare-earth element (REE) patterns for observed and modeled daughter magmas in fractional crystallization models. Differentiation pathways include (A) low-Mg andesite to dacite, (B) magnesian andesite to dacite, and (C) dacite to rhyolite. The gray dashed line in (A) represents the REE pattern calculated for fractional crystallization of 1.5% apatite using the partition coefficients of Prowatke and Klemme (2006). The black dashed line in (B) represents REE data for the same magnesian andesite sample (DR25-1) reported during a different analytical campaign by Hauff et al. (2021). Calculated trends follow the Rayleigh fractionation model, with parameters listed in Table S2. Normalizing values are from McDonough and Sun (1995). Fractional crystallization of magnesian andesites better reproduces both major and REE compositions of dacites compared to low-Mg andesites.

during 70% crystal fractionation, modeled under specific conditions (initial 3.0 wt.% H_2O, 3.0 kbar, ΔQFM +1). MELTS calculations produced liquids with significantly lower FeO*/MgO, TiO_2, and FeO* values compared to observed trends in the Kibblewhite magmas, which can be attributed to the premature crystallization of Fe-Ti oxides. To address this, the COMAGMAT model was used with corrected liquidus temperatures for Fe-Ti oxides, resulting in compositional trends

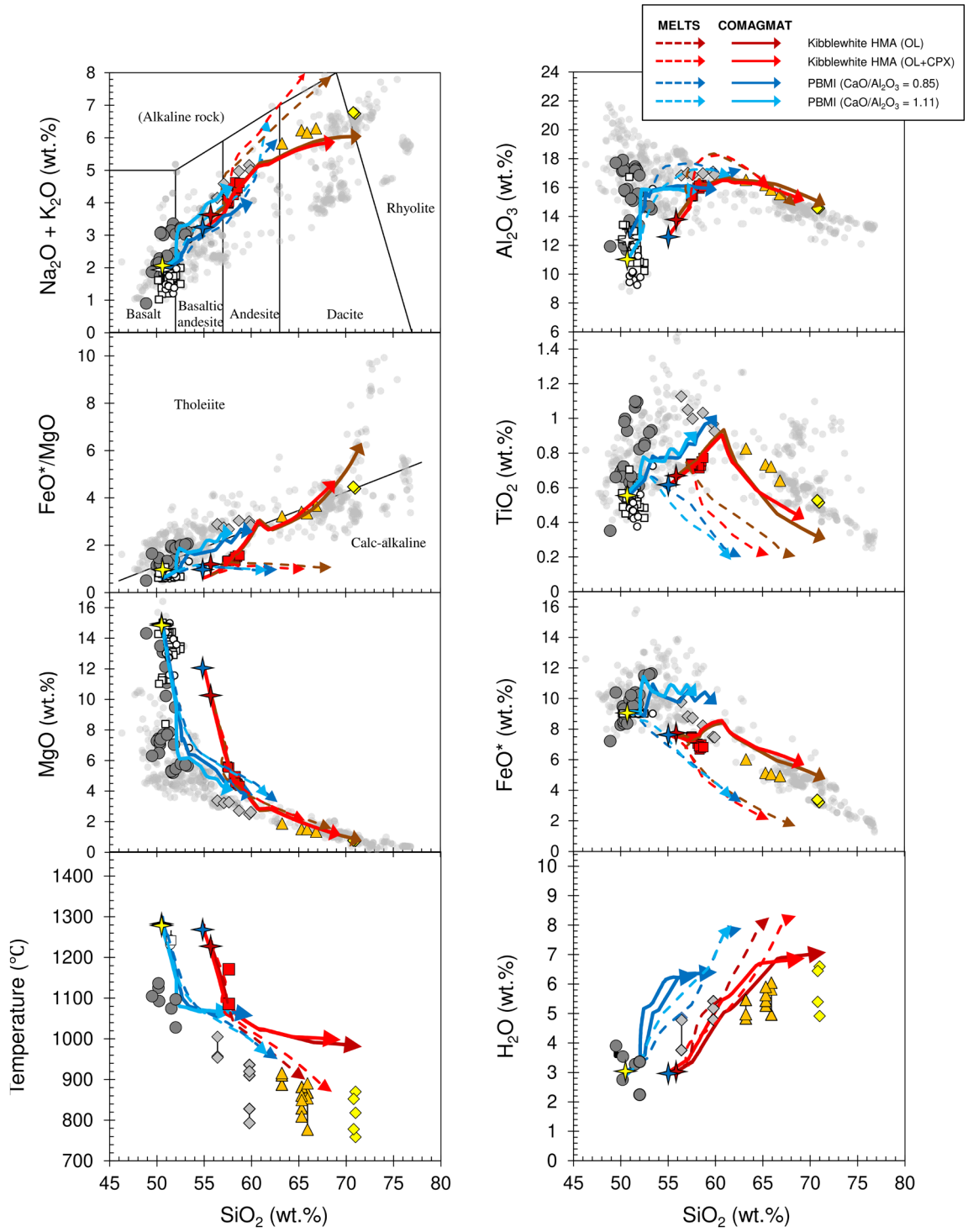

FIGURE 5 | Thermodynamic fractional crystallization modeling of primary magmas using rhyolite-MELTS and COMAGMAT. Results show compositional changes during 70% crystal fractionation starting from Kibblewhite HMAs and PBMIs. Andesitic primary magmas produce rhyolitic melts, while basaltic primary magmas yield andesitic compositions. The models assume an initial H_2O content of 3.0 wt.%, isobaric crystallization at 3 kbar, and an oxidation state constrained at ΔQFM +1.

more consistent with the magmatic variations observed in the Kibblewhite Volcano.

The most notable distinction between the HMA and PBMI differentiation models lies in the SiO_2 content of the resulting liquids. After 70% crystal fractionation, Kibblewhite HMAs produced rhyolitic liquids, whereas PBMIs yielded only andesitic liquids (Figure 4). Although variations in modeling conditions (pressure, water content, and oxygen fugacity) caused slight differences in differentiation pathways, the SiO_2 contents of the final liquids in the HMA differentiation model (65–72 wt.% SiO_2) consistently remained higher than those in the basalt differentiation

model (50–63 wt.% SiO_2) (Figure S8). These findings suggest that PBMIs cannot produce rhyolitic melts through ~70% crystallization, but the HMAs can.

5 | Discussion

5.1 | Origin of Silicic Magmas in the Kibblewhite Volcano

This section examines the origin of silicic magmas at the Kibblewhite Volcano by evaluating two alternative differentiation models: fractional crystallization of primary basaltic magmas producing low-Mg andesites, and fractional crystallization of primary andesitic magmas represented by magnesian andesites. We assess these models using constraints from magmatic conditions, chemical compositions, and crystallization efficiency, and evaluate their respective abilities to account for the observed dacitic to rhyolitic magmas.

5.1.1 | Constraints From Magmatic Conditions and Chemical Compositions

Low-Mg andesites record temperatures similar to or slightly higher than those of dacites and rhyolites (800°C–1000°C) and similarly high H_2O contents (4.0–6.0 wt.%), indicating that they represent already evolved magmas rather than primitive parental melts. This interpretation is supported by mass-balance calculations, which show that the REE compositions of dacites and rhyolites cannot be reproduced by further fractional crystallization of low-Mg andesites. The discrepancy of REE patterns between the low-Mg andesites and dacites can possibly be explained by the fractionation of potential accessory minerals, such as apatite; however, inclusion of a minor amount of apatite fractionation improves the fit for the heavy REE, but the overall REE patterns of the dacites remain inconsistent with those predicted from low-Mg andesite parental compositions (Figure 4A).

By contrast, magnesian andesites provide a closer match to both the major-element and REE compositions of the dacites and rhyolites, suggesting that fractional crystallization of magnesian andesitic magmas offers a more consistent explanation for the generation of silicic melts at the Kibblewhite Volcano. The weak negative Eu anomaly observed in the magnesian andesites warrants careful consideration, but we do not consider that this negative Eu anomaly necessarily implies magma mixing or crustal plagioclase fractionation for the following reasons. First, comparison of replicate analyses of the same magnesian andesite sample (DR25-1) obtained during different analytical campaigns indicates that the magnitude of the Eu anomaly is modest (Eu/Eu*≈0.8–0.9; Figure 4B). Second, a weak negative Eu anomaly may arise during mantle melting under low-pressure conditions where plagioclase is stable (Tamura et al. 2019). The Kibblewhite HMA may have formed in the shallow mantle (~1.0 GPa) beneath the thin crust of the Kermadec arc (Hirai et al. 2023), where plagioclase can be stable in peridotite. Alternatively, it may arise through kinetic and disequilibrium processes involving clinopyroxene during mantle melting (Tilhac et al. 2023). Hirai et al. (2024) proposed that the magnesian andesites originated from a harzburgitic mantle source produced by reaction between peridotite and primitive basaltic melts. The absence of clinopyroxene in the melting assemblage possibly contributes to the weak negative Eu anomaly. Thus, we consider that the Eu anomaly in the magnesian andesites is best interpreted as reflecting mantle melting processes rather than providing a direct link to silicic magma mixing.

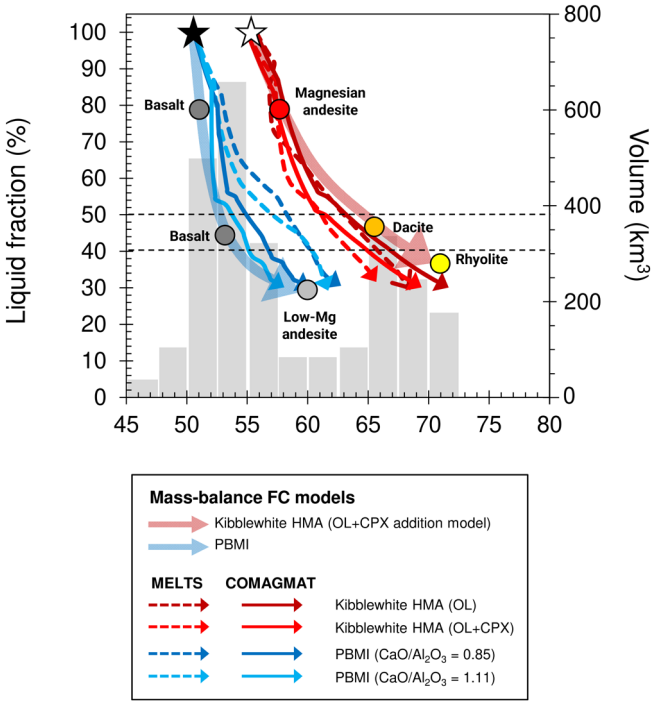

FIGURE 6 | SiO_2 versus remaining liquid fractions for the basalt and HMA differentiation models. Filled and open stars denote SiO_2 contents of PBMIs and Kibblewhite HMAs, respectively. Gray Volume-weighted SiO_2 histogram of magmatic ejecta from Kermadec arc (Wright et al. 2006).

5.1.2 | Constraints From Magmatic Volume

Mass-balance and thermodynamic modeling provide additional constraints on the origin of silicic magmas at the Kibblewhite Volcano. The models indicate that approximately 50%–60% fractional crystallization of magnesian andesitic magmas can generate dacitic melts, whereas a similar degree of crystallization applied to primitive basaltic magmas results in basalt to basaltic andesite compositions (Figure 6). This contrast reflects the mineralogy of the fractionating assemblage (olivine, clinopyroxene, and plagioclase), which typically contains ~50 wt.% SiO_2. Fractionation of such phases from basaltic magmas with comparable SiO_2 contents therefore produces limited increases in melt SiO_2, whereas andesitic magmas (> 55 wt.% SiO_2) can evolve toward dacitic compositions during continued crystallization (see Figure 11 in Kelemen et al. 2003). Of course, basaltic magmas can ultimately generate rhyolitic melts given sufficiently extensive differentiation. However, here we emphasize differences in the relative efficiency of SiO_2 enrichment during the differentiation process.

Thus, primary andesitic magmas are more efficient than basaltic magmas at generating silicic melts. As crystallization efficiency alone does not uniquely identify the parental magma of the silicic compositions, magmatic volume considerations should be regarded as complementary to the geochemical and petrological constraints discussed above. However, the fact that these two primary magmas can produce two distinct differentiated magma series—low-Mg andesites and dacites—through comparable degrees of fractional crystallization has important implications. In general, magmas reaching crystallinities of ~50–60 vol.% are commonly interpreted to transition toward crystal mush behavior and enter a "rheological lock-up" state, resulting in storage within the crust (Bachmann and Bergantz 2008; Marsh 1981). If primary basaltic and andesitic magmas each independently formed crystal mush, and the extracted melts correspond to the low-Mg andesites and dacites, respectively. This framework possibly accounts for the coexistence of the two differentiated magma series at the Kibblewhite Volcano.

5.1.3 | Two Differentiation Pathways at the Kibblewhite Volcano

The results presented above suggest that magmatic differentiation at the Kibblewhite Volcano could not be explained by a single evolutionary pathway, but instead imply the coexistence of two distinct differentiation pathways. One pathway involves fractional crystallization of primary basaltic magmas, producing low-Mg andesites. These magmas represent already evolved compositions and cannot account for the chemical characteristics of the dacites through further crystallization. The other pathway involves fractional crystallization of primary andesitic magmas, represented by magnesian andesites, which successfully reproduce the major- and trace-element compositions of the dacites. In the following section, we evaluate whether this framework can be extended to bimodal volcanism in the Kermadec arc.

5.2 | Implications for Bimodal Volcanism in the Kermadec Arc

Previous studies have proposed that rhyolitic magmas in the Kermadec arc can be generated through extensive (70%–80%) fractional crystallization of basaltic magmas (Haase et al. 2006; Barker et al. 2013; Keith et al. 2018; Knafelc et al. 2022). However, these models employ parental basalt compositions that are not strictly primitive (5.4–7.5 wt.% MgO and FeO*/MgO = 1.2–2.2), indicating that some degree of differentiation had already occurred. As a result, the efficiency of rhyolite generation inferred in these studies may reflect the use of evolved starting compositions rather than primary basaltic melts.

The Kibblewhite Volcano indicates that basaltic and andesitic primary magmas may follow parallel differentiation pathways within a single volcanic system. In the Kermadec arc, primary magmas are expected to range from basaltic to andesitic compositions as a result of mantle melting over a range of pressures. Thus, the 50%–60% parallel differentiation of mantle-derived basaltic and andesitic magmas may provide a potential explanation for the bimodal SiO_2 distribution observed in the arc (Figure 6). In this section, we examine whether the two differentiation pathways identified at the Kibblewhite Volcano can be distinguished elsewhere in the Kermadec arc, and we compare these trends with those observed in the Izu arc, another oceanic arc characterized by bimodal magmatism.

5.2.1 | Discrimination of the Two Differentiation Pathways

Here, we propose that the FeO*/MgO–SiO_2 diagram, which has traditionally been used to classify magmatic series, is also useful for distinguishing between the two differentiation pathways. When the Kibblewhite data are plotted on the FeO*/MgO–SiO_2 diagram, ankaramites, basalts, and low-Mg andesites form a coherent "basalt differentiation series", whereas magnesian andesites, dacites, and rhyolites form a separate "andesite differentiation series" (Figure 7A). These two series could not be adequately distinguished using the traditional discrimination line of Miyashiro (1974), as both exhibit tholeiitic differentiation trends originating from primary magmas. This limitation arises because the Miyashiro diagram implicitly assumes that volcanic arcs are supplied exclusively by basaltic primary magmas, and therefore does not account for the coexistence of basaltic and andesitic primary melts, such as observed at the Kibblewhite Volcano. We therefore define a new discrimination boundary on the FeO*/MgO–SiO_2 diagram, hereafter referred to as the Kibblewhite discrimination line (dashed line in Figure 7A), based on the two differentiation trends observed at the Kibblewhite Volcano.

To test the broader applicability, we applied this discrimination to other volcanic arcs where silicic magmas are generated through differentiation of basaltic or andesitic primary magmas. When applied to the Ogasawara boninite suite (Taylor et al. 1994), boninites and associated silicic rocks plot within the andesite differentiation series (Figure 7B). This supports the interpretation that the Kibblewhite silicic magmas can be derived from high-Mg andesitic primary magmas. In contrast, application of the Kibblewhite discrimination line to the Monowai Volcano in the Kermadec arc (Timm et al. 2012) and Western Epi in the Vanuatu Arc (Barsdell and Berry 1990) indicates that the differentiation trends observed in these volcanic systems correspond to the basalt differentiation series (Figure 7B). Barsdell and Berry (1990) estimated that the dacite of the Western Epi Volcano in the Vanuatu arc (68 wt.% SiO_2; FeO*/MgO = 8.4) was produced by ~90% fractional crystallization of the primitive ankaramites. Timm et al. (2012) estimated the dacite of the Monowai Volcano (63 wt.% SiO_2; FeO*/MgO = 8.2) was produced by ~80% fractional crystallization of the coeval basalt. These dacites are characterized by relatively high FeO*/MgO ratios, suggesting that they may be distinguished from dacites derived from andesitic primary magmas, such as those associated with boninitic systems. These examples support the interpretation of this study that silicic magmas can be generated through fractional crystallization of basaltic magmas, but typically require highrt degrees of crystallization.

Thus, the two differentiation trends identified at the Kibblewhite Volcano may also provide a means to distinguish magmatic series derived from basaltic and andesitic primary magmas at other volcanic systems. In the following section, we examine

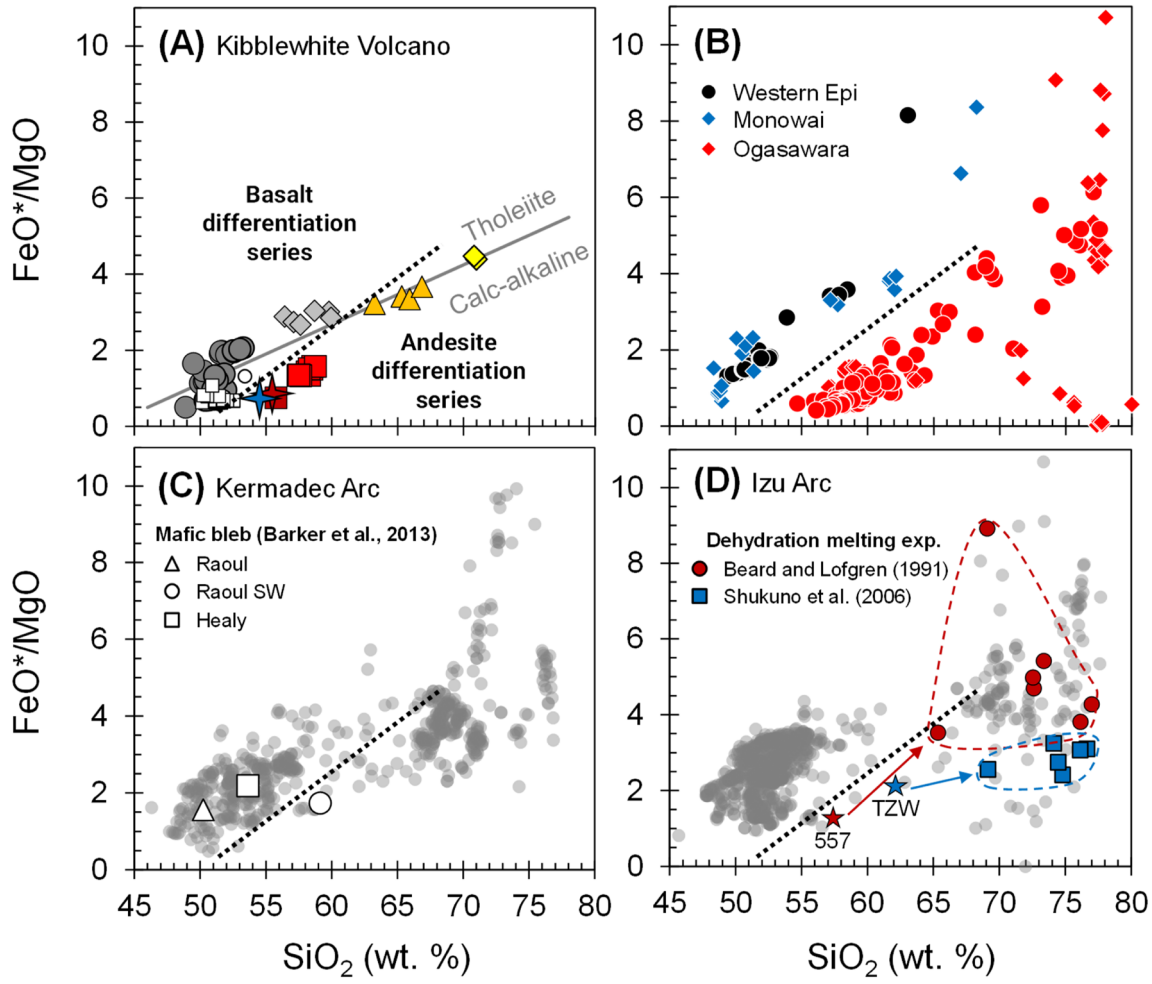

FIGURE 7 | New FeO*/MgO–SiO_2 discrimination diagrams. (A) Newly defined Kibblewhite discrimination line (dashed line) derived from the two differentiation series identified at the Kibblewhite Volcano. The solid gray line represents the traditional Miyashiro boundary separating tholeiitic and calc-alkaline series (Miyashiro 1974). The symbols and data sources are the same as that in Figure 1. (B) Application of the new discrimination line to magmatic series generated by differentiation of primary basaltic and primary andesitic magmas. The black circles and blue diamonds represent the whole-rock compositions of Western Epi volcanic rocks in the Vanuatu arc (Barsdell and Berry 1990) and the Monowai Volcanic Center in the Kermadec arc (Timm et al. 2012), respectively. The red circles and diamonds indicate whole-rock and glass compositions of boninites from the Ogasawara Islands in the proto-Ogasawara Arc (Kanayama et al. 2012; Taylor et al. 1994; Umino 1986), respectively. (C) Application of the new discrimination line to the Kermadec arc. The open symbols represent compositions of mafic blebs that have been identified as interacting with silicic magmas at Kermadec arc volcanoes (Barker et al. 2013). The data sources are the same as that in Figure 1. (D) Application of the new discrimination line to the Izu arc. The data were sourced from the GEOROC Database. The red circles and blue squares represent the compositions of partial melts from dehydration melting experiments of magnesian andesite composition (sample 557) (Beard and Lofgren 1991) and tonalite from the Tanzawa Plutonic Complex (TZM) (Shukuno et al. 2006), respectively.

the implications of applying this discrimination to the entire Kermadec arc.

5.2.2 | Implications for the Kermadec Arc and Comparison With the Izu Arc

Figure 7C illustrates the application of the Kibblewhite discrimination line to the entire Kermadec arc. Differentiation trends across the arc do not separate into two clearly defined pathways along the discrimination line, largely because andesites from the Kermadec arc display a wide range of FeO*/MgO ratios, overlapping both the basalt and andesite differentiation series. One possible explanation for this compositional spread is magma mixing between basaltic and dacitic melts. Mafic blebs observed at several Kermadec volcanoes, including Raoul Island, provide clear evidence for interaction between basaltic and silicic magmas within the crust (Barker et al. 2013). Such interaction, however, does not necessarily establish a direct parental relationship between the two magmas. Even if silicic melts were initially derived from primary andesitic magmas, basaltic magmas ascending from separate sources could plausibly interact with shallow silicic reservoirs prior to eruption, producing the petrographic and geochemical features documented at volcanoes such as Raoul.

An alternative explanation is the coexistence of two differentiation pathways derived from distinct primary magmas, as observed at the Kibblewhite Volcano. If primary andesitic magmas are also generated beneath other Kermadec arc volcanoes,

their fractional crystallization could account for the presence of andesites to dacites with relatively low FeO*/MgO ratios. Moreover, the differentiation trends defined by dacites and rhyolites resemble those of the Ogasawara boninites, further supporting a differentiation model involving primary andesitic magmas. Accordingly, we suggest that the two differentiation pathways identified at the Kibblewhite Volcano may also be applicable to understanding magmatic evolution across the Kermadec arc.

Furthermore, the possibility that silicic magmas in the Kermadec arc evolved from primary andesitic magmas is also supported by comparison with the Izu arc. Figure 7D shows the application of the Kibblewhite discrimination line to the Izu arc, another oceanic arc characterized by bimodal volcanism of basaltic and rhyolitic magmas (Tamura and Tatsumi 2002). The magmatic variation of the Izu arc closely resembles that of the Kermadec arc and appears to be distinguishable into a continuous basalt differentiation series extending from basalts and an andesite differentiation series represented by dacites. However, the processes responsible for generating rhyolitic magmas could be different between the two arcs. Silicic magmas in the Izu arc have commonly been interpreted as products of dehydration melting of the andesitic middle crust, based on several petrographic and geochemical observations (Shukuno et al. 2006; Tamura et al. 2009). These include: (1) the presence of reversely zoned orthopyroxene phenocrysts, which have been attributed to pre-eruptive heating; (2) matrix glass compositions that are comparable to partial melts produced in experimental dehydration melting of andesite (Beard and Lofgren 1991; Shukuno et al. 2006); and (3) phenocryst assemblages consistent with the residual mineral phases of such experiments (clinopyroxene + orthopyroxene + plagioclase + magnetite ± quartz). In contrast, dacites and rhyolites from the Kermadec arc exhibit petrographic characteristics that differ from those observed in the Izu arc, including (1) a relative scarcity of mineralogical disequilibrium features and (2) the presence of amphibole phenocrysts. These observations suggest that silicic magmas in the Kermadec arc are more plausibly explained by fractional crystallization, rather than by anatexis of andesitic crust.

Although the mechanisms responsible for generating silicic magmas in the Kermadec and Izu arcs may therefore differ, their compositional similarities suggest that they could be linked to andesitic source materials. Notably, the andesitic starting composition (557) used in the dehydration melting experiments of Beard and Lofgren (1991) is chemically similar to the magnesian andesites from the Kibblewhite Volcano, and the melts produced in these experiments overlap compositionally with silicic magmas from both the Izu and Kermadec arcs (Figure 7). In addition, melting experiments on the Tanzawa tonalite, an andesitic composition exposed in the collision zone between the Izu and the Honshu arc, have been shown to produce melts with compositions similar to the Izu rhyolites (Shukuno et al. 2006). Experimental studies have shown that melt compositions generated by dehydration melting can be similar to those produced by fractional crystallization under comparable temperature and pressure conditions (e.g., Tatsumi and Suzuki 2009). Thus, these observations raise the possibility that silicic magmas in both arcs may ultimately be derived from magnesian andesitic compositions.

Silicic magmas in the Kermadec arc have commonly been attributed to fractional crystallization of basaltic magmas, and this study does not seek to replace that model. At the same time, there is no compelling reason to exclude the possibility that some silicic magmas in the Kermadec arc could be derived from primary andesitic magmas. To further strengthen the andesite differentiation model, several unresolved issues need to be addressed, and these are discussed in the following section.

5.2.3 | Do Primary Andesitic Magmas Occur in the Kermadec Arc?

A fundamental limitation of the andesite differentiation model is that it requires the presence of primary andesitic magmas, which have so far been clearly identified only at the Kibblewhite Volcano within the Kermadec arc. In fact, regardless of the degree of differentiation, eruptions of andesitic magma are rare throughout the Kermadec arc (Figure 6). The Kermadec arc is characterized by a thin crust (~15 km; Bassett et al. 2016), under which melting of the shallow upper mantle could plausibly generate primary andesitic magmas (Tamura et al. 2016). This raises the question of why (primary) andesitic magmas are rarely observed in the Kermadec arc.

One possible explanation for the apparent scarcity of primary andesitic magmas may reflect sampling bias associated with dredging focused on volcanic summits. It has been known that primitive magmas may bypass main magma chambers and erupt near the base of volcanic edifices (Tamura et al. 2014). In fact, differentiated magmas (low-Mg andesite, dacites, rhyolites) were collected near the summit at the Kibblewhite Volcano (Figure 1). On the other hand, magnesian andesites were collected from a small fissure vent at the foot of the Kibblewhite Volcano. Basalts, including ankaramites, have also been sampled from relatively small satellite cones. These observations suggest that highly evolved magmas may be preferentially distributed near the summits of large volcanic edifices. Consequently, primary magmas may be difficult to identify within the main bodies of large, well-defined volcanoes that have been the primary targets of seafloor morphological surveys.

Another possibility is that primary magmas are inherently difficult to erupt to the surface. Importantly, the scarcity applies not only to primary andesitic magmas but also to primary basaltic magmas within the arc. Even the basaltic magmas that are dominant in the Kermadec arc are mostly evolved, as indicated by their high FeO*/MgO ratios (> 1.0), suggesting that truly primitive magmas are rarely preserved. An exception may be the ankaramites recovered from the Kibblewhite Volcano, which have been interpreted as primary basaltic magmas based on melt inclusion studies (Hirai et al. 2024), despite containing exceptionally high proportions of olivine and clinopyroxene crystals (Figure S1). Pressure estimates derived from clinopyroxene megacrysts in these ankaramites (~0.5 GPa; Figure 3) indicate that crystallization commenced near the crust–mantle boundary, implying that primary basaltic magmas began to crystallize shortly after generation. Although the ankaramites experienced decompression- and cooling-induced crystallization during ascent, they appear to have erupted without significant crystal–liquid segregation, possibly because their basaltic composition

results in relatively low melt viscosity. If such ankaramite magmas failed to erupt and instead formed crystal mushes with ~50–60 vol.% crystallinities, the interstitial melts extracted from these mushes would be expected to have basaltic to basaltic andesite compositions (SiO_2 = 50–55 wt.%; Figure 6). Thus, eruption of such extracted melts could account for the lower SiO_2 peaks observed in the bimodal volcanism of the Kermadec arc.

Even if primary andesitic magmas are generated, crystallization within the crust would similarly be unavoidable, making it difficult for such magmas to erupt in an undifferentiated state. In particular, because magma viscosity strongly depends on SiO_2 content (Giordano et al. 2008; Shaw 1972), primary andesitic magmas are expected to be more viscous than basaltic magmas and more difficult to erupt. If primary andesitic magmas form crystal mushes with ~50–60 vol.% crystallinities, the extracted interstitial melts would be dacitic to rhyolitic in composition, and their eruption could account for the higher SiO_2 peak observed in the bimodal magmatism of the Kermadec arc (Figure 6). In this framework, the coexistence of basaltic and andesitic primary magmas, each forming crystal mushes and generating differentiated melts, provides a plausible explanation for both the bimodal SiO_2 distribution and the relative scarcity of erupted andesites in the arc. From this perspective, primary andesitic melts may not be absent in the Kermadec arc but instead may rarely reach the surface owing to inevitable crystallization during ascent and storage. Accordingly, the apparent rarity of (primary) andesitic magmas does not invalidate the andesite differentiation model; further progress requires direct evidence for primary andesitic melts, such as that preserved in melt inclusions within early-crystallized minerals.

6 | Conclusion

This study shows that silicic magmas at the Kibblewhite Volcano are best explained by the coexistence of two differentiation pathways involving compositionally distinct primary magmas. An important implication is that the silicic magmas at Kibblewhite are more plausibly derived from independent differentiation of primary andesitic magmas than from the low-Mg andesites. The Kibblewhite Volcano provides an example demonstrating that basaltic and andesitic primary magmas can evolve in parallel within a single oceanic arc volcano. This finding highlights the importance of considering multiple primary magma compositions when interpreting the origin of silicic magmas in oceanic arcs characterized by thin crust.

While this framework may have broader relevance for understanding bimodal volcanism in the Kermadec arc, its applicability beyond Kibblewhite remains to be tested. In particular, direct evidence for primary magmas at other volcanic centers will be essential for evaluating whether similar differentiation pathways operate elsewhere. Accordingly, the interpretation presented here is intended as a testable working hypothesis rather than a general model for the entire arc.

Acknowledgments

This work was supported by JSPS KAKENHI Grant Nos. 19J10691 and 24H02520 to Y.H. and Grant No. JP21H01195 to Y.T. Part of this research was supported by the Environment Research and Technology Development Fund (Grant No. JPMEERF20244M02) of the Environmental Restoration and Conservation Agency, provided by the Ministry of the Environment of Japan. We thank Christpher Conway and Simon Barker for their insightful reviews. We would like to thank Editage (www.editage.jp) for the English language editing.

Funding

This work was supported by JSPS KAKENHI Grant Nos. 19J10691 and 24H02520 to Y.H. and Grant No. JP21H01195 to Y.T. Part of this research was supported by the Environment Research and Technology Development Fund (Grant No. JPMEERF20244M02) of the Environmental Restoration and Conservation Agency, provided by the Ministry of the Environment of Japan.

Ethics Statement

The authors have nothing to report.

Conflicts of Interest

The authors declare no conflicts of interest.

Data Availability Statement

All data generated or analyzed during this study are included in this published article and its Supporting Information files.

References

Arató, R., and A. Audétat. 2017. "FeTiMM—A New Oxybarometer for Mafic to Felsic Magmas." *Geochemical Perspectives Letters* 5: 19–23. https://doi.org/10.7185/geochemlet.1740.

Ariskin, A. A., and G. S. Barmina. 2004. "COMAGMAT: Development of a Magma Crystallization Model and Its Petrological Applications." *Geochemistry International* 42, no. Suppl: S1–S157.

Bachmann, O., and G. W. Bergantz. 2008. "Rhyolites and Their Source Mushes Across Tectonic Settings." *Journal of Petrology* 49, no. 12: 2277–2285. https://doi.org/10.1093/petrology/egn068.

Barker, S. J., C. J. N. Wilson, J. A. Baker, et al. 2013. "Geochemistry and Petrogenesis of Silicic Magmas in the Intra-Oceanic Kermadec Arc." *Journal of Petrology* 54, no. 2: 351–391. https://doi.org/10.1093/petrology/egs071.

Barsdell, M., and R. F. Berry. 1990. "Origin and Evolution of Primitive Island Arc Ankaramites From Western Epi, Vanuatu." *Journal of Petrology* 31: 747–777.

Bassett, D., H. Kopp, R. Sutherland, et al. 2016. "Crustal Structure of the Kermadec Arc From MANGO Seismic Refraction Profiles." *Journal of Geophysical Research: Solid Earth* 121, no. 10: 7514–7546. https://doi.org/10.1002/2016JB013194.

Beard, J. S., and G. E. Lofgren. 1991. "Dehydration Melting and Water-Saturated Melting of Basaltic and Andesitic Greenstones and Amphibolites at 1, 3, and 6. 9 Kb." *Journal of Petrology* 32, no. 2: 365–401. https://doi.org/10.1093/petrology/32.2.365.

Bédard, J. H. 2006. "Trace Element Partitioning in Plagioclase Feldspar." *Geochimica et Cosmochimica Acta* 70, no. 14: 3717–3742. https://doi.org/10.1016/j.gca.2006.05.003.

Brophy, J. G. 2008. "A Study of Rare Earth Element (REE)-SiO2 Variations in Felsic Liquids Generated by Basalt Fractionation and Amphibolite Melting: A Potential Test for Discriminating Between the Two Different Processes." *Contributions to Mineralogy and Petrology* 156, no. 3: 337–357. https://doi.org/10.1007/s00410-008-0289-x.

Cabero, M. T., S. Mecoleta, and F. J. López-Moro. 2012. "OPTIMASBA: A Microsoft Excel Workbook to Optimise the Mass-Balance Modelling

Applied to Magmatic Differentiation Processes and Subsolidus Overprints." *Computers and Geosciences* 42: 206–211. https://doi.org/10.1016/j.cageo.2011.10.013.

Carey, R. J., R. Wysoczanski, R. Wunderman, and M. Jutzeler. 2014. "Discovery of the Largest Historic Silicic Submarine Eruption." *Eos, Transactions American Geophysical Union* 95, no. 19: 157–159. https://doi.org/10.1002/2014EO190001.

Ewart, A., W. B. Bryan, B. W. Chappell, and R. L. Rudnick. 1994. "24. Regional Geochemistry of the Lau-Tonga Arc and Backarc Systems." *Proceeding of the Ocean Drilling Program, Scientific Results* 135: 385–425.

Gamble, J., J. O. N. Woodhead, I. A. N. Wright, and I. A. N. Smith. 1996. "Basalt and Sediment Geochemistry and Magma Petrogenesis in a Transect From Oceanic Island Arc to Rifted Continental Margin Arc: The Kermadec-Hikurangi Margin, SW Pacific." *Journal of Petrology* 37, no. 6: 1529–1546.

Gamble, J. A., R. H. K. Christie, I. C. Wright, and R. J. Wysoczanski. 1997. "Primitive K-Rich Magmas From Clark Volcano, Southern Kermadec Arc; a Paradox in the K-Depth Relationship." *Canadian Mineralogist* 35, no. 2: 275–290.

Gamble, J. A., I. E. M. Smith, M. T. McCulloch, I. J. Graham, and B. P. Kokelaar. 1993. "The Geochemistry and Petrogenesis of Basalts From the Taupo Volcanic Zone and Kermadec Island Arc, S.W. Pacific." *Journal of Volcanology and Geothermal Research* 54, no. 3–4: 265–290. https://doi.org/10.1016/0377-0273(93)90067-2.

Gamble, J. A., I. C. Wright, and J. A. Baker. 1993. "Seafloor Geology and Petrology in the Oceanic to Continental Transition Zone of the Kermadec-Havre-Taupo Volcanic Zone Arc System, New Zealand." *New Zealand Journal of Geology and Geophysics* 36, no. 4: 417–435. https://doi.org/10.1080/00288306.1993.9514588.

Ghiorso, M. S., and G. A. R. Gualda. 2015. "An H2O–CO2 Mixed Fluid Saturation Model Compatible With Rhyolite-MELTS." *Contributions to Mineralogy and Petrology* 169, no. 6: 1–30. https://doi.org/10.1007/s00410-015-1141-8.

Giordano, D., J. K. Russell, and D. B. Dingwell. 2008. "Viscosity of Magmatic Liquids: A Model." *Earth and Planetary Science Letters* 271, no. 1–4: 123–134. https://doi.org/10.1016/j.epsl.2008.03.038.

Haase, K. M., S. Krumm, M. Regelous, M. Joachimski, and R. Isl. 2011. "Oxygen Isotope Evidence for the Formation of Silicic Kermadec Island Arc and Havre—Lau Backarc Magmas by Fractional Crystallisation." *Earth and Planetary Science Letters* 309, no. 3–4: 348–355. https://doi.org/10.1016/j.epsl.2011.07.014.

Haase, K. M., N. Stroncik, D. Garbe-Schönberg, and P. Stoffers. 2006. "Formation of Island Arc Dacite Magmas by Extreme Crystal Fractionation: An Example From Brothers Seamount, Kermadec Island Arc (SW Pacific)." *Journal of Volcanology and Geothermal Research* 152, no. 3–4: 316–330. https://doi.org/10.1016/j.jvolgeores.2005.10.010.

Haase, K. M., T. J. Worthington, P. Stoffers, D. Garbe-scho, and I. Wright. 2002. "Mantle Dynamics, Element Recycling, and Magma Genesis Beneath the Kermadec Arc-Havre Trough." *Geochemistry, Geophysics, Geosystems* 3, no. 11: 1–22. https://doi.org/10.1029/2002GC000335.

Hauff, F., K. Hoernle, J. Gill, et al. 2021. *R/V SONNE Cruise SO255 "VITIAZ": An Integrated Major Element, Trace Element and Sr-Nd-Pb-Hf Isotope Data Set of Volcanic Rocks From the Colville and Kermadec Ridges, the Quaternary Kermadec Volcanic Front and the Havre Trough Backarc Basin, Version 1.0*. Interdisciplinary Earth Data Alliance (IEDA). https://doi.org/10.26022/IEDA/111723.

Hirai, Y., Y. Tamura, T. Hanyu, Q. Chang, C. Timm, and K. Hoernle. 2024. "Why Are Oceanic Arc Basalts ca-Rich and Ni-Poor? Insights From Olivine-Hosted Melt Inclusions From Kibblewhite Volcano in the Kermadec Arc." *Chemical Geology* 662: 122218. https://doi.org/10.1016/j.chemgeo.2024.122218.

Hirai, Y., Y. Tamura, T. Sato, et al. 2023. "Magnesian Andesites From Kibblewhite Volcano in the Kermadec Arc, New Zealand." *Journal of Petrology* 64, no. 9: 1–23. https://doi.org/10.1093/petrology/egad060.

Jutzeler, M., R. Marsh, R. J. Carey, J. D. L.White, P. J. Talling, and L. Karlstrom. 2014. "On the Fate of Pumice Rafts Formed During the 2012 Havre Submarine Eruption." *Nature Communications* 5, no. 1: 3660. https://doi.org/10.1038/ncomms4660.

Kanayama, K., S. Umino, and O. Ishizuka. 2012. "Eocene Volcanism During the Incipient Stage of Izu-Ogasawara Arc: Geology and Petrology of the Mukojima Island Group, the Ogasawara Islands." *Island Arc* 21, no. 4: 288–316. https://doi.org/10.1111/iar.12000.

Keith, M., K. M. Haase, R. Klemd, D. J. Smith, U. Schwarz-Schampera, and W. Bach. 2018. "Constraints on the Source of cu in a Submarine Magmatic-Hydrothermal System, Brothers Volcano, Kermadec Island Arc." *Contributions to Mineralogy and Petrology* 173, no. 5: 1–16. https://doi.org/10.1007/s00410-018-1470-5.

Kelemen, P. B., K. Hanghøj, and A. R. Greene. 2003. "One View of the Geochemistry of Subduction-Related Magmatic Arcs, With an Emphasis on Primitive Andesite and Lower Crust." In *Treatise on Geochemistry*, vol. 3–9, 2–70. Elsevier Inc. https://doi.org/10.1016/B0-08-043751-6/03035-8.

Knafelc, J., S. E. Bryan, D. Gust, and H. E. Cathey. 2020. "Defining Pre-Eruptive Conditions of the Havre 2012 Submarine Rhyolite Eruption Using Crystal Archives." *Frontiers in Earth Science* 8: 549715. https://doi.org/10.3389/feart.2020.00310.

Knafelc, J., D. Gust, S. E. Bryan, M. Anderson, and H. E. Cathey. 2022. "Petrogenesis of Havre Volcano in the Kermadec Arc: 2012 Eruption of a Chemically Homogeneous Rhyolite." *Frontiers in Earth Science* 10: 1. https://doi.org/10.3389/feart.2022.886897.

Lepage, L. D. 2003. "ILMAT: An Excel Worksheet for Ilmenite-Magnetite Geothermometry and Geobarometry." *Computers and Geosciences* 29, no. 5: 673–678. https://doi.org/10.1016/S0098-3004(03)00042-6.

Lynett, P., M. McCann, Z. Zhou, et al. 2022. "Diverse Tsunamigenesis Triggered by the Hunga Tonga-Hunga Ha'apai Eruption." *Nature* 609, no. 7928: 728–733. https://doi.org/10.1038/s41586-022-05170-6.

Marsh, B. D. 1981. "On the Crystallinity, Probability of Occurrence, and Rheology of Lava and Magma." *Contributions to Mineralogy and Petrology* 78, no. 1: 85–98. https://doi.org/10.1007/BF00371146.

McDonough, W. F., and S.-s. Sun. 1995. "The Composition of the Earth." *Chemical Geology* 120: 223–253.

Miyashiro, A. 1974. "Volcanic Rock Series in Island Arcs and Active Continental Margins." *American Journal of Science* 274, no. 4: 321–355. https://doi.org/10.2475/ajs.274.4.321.

Nandedkar, R. H., N. Hürlimann, P. Ulmer, and O. Müntener. 2016. "Amphibole–Melt Trace Element Partitioning of Fractionating Calc-Alkaline Magmas in the Lower Crust: An Experimental Study." *Contributions to Mineralogy and Petrology* 171, no. 8–9: 1–25. https://doi.org/10.1007/s00410-016-1278-0.

Nielsen, R. L., W. E. Gallahan, and F. Newberger. 1992. "Experimentally Determined Mineral-Melt Partition Coefficients for Sc, Y and REE for Olivine, Orthopyroxene, Pigeonite, Magnetite and Ilmenite." *Contributions to Mineralogy and Petrology* 110, no. 4: 488–499. https://doi.org/10.1007/BF00344083.

Prowatke, S., and S. Klemme. 2006. "Trace Element Partitioning Between Apatite and Silicate Melts." *Geochimica et Cosmochimica Acta* 70, no. 17: 4513–4527. https://doi.org/10.1016/j.gca.2006.06.162.

Putirka, K. 2016. "Amphibole Thermometers and Barometers for Igneous Systems and Some Implications for Eruption Mechanisms of Felsic Magmas at Arc Volcanoes." *American Mineralogist* 101, no. 4: 841–858. https://doi.org/10.2138/am-2016-5506.

Putirka, K. D. 2008. "Thermometers and Barometers for Volcanic Systems." *Reviews in Mineralogy and Geochemistry* 69: 61–120. https://doi.org/10.2138/rmg.2008.69.3.

Ridolfi, F. 2021. "Amp-tb2: An Updated Model for Calcic Amphibole Thermobarometry." *Minerals* 11, no. 3: 1–9. https://doi.org/10.3390/min11030324.

Ridolfi, F., and A. Renzulli. 2012. "Calcic Amphiboles in Calc-Alkaline and Alkaline Magmas: Thermobarometric and Chemometric Empirical Equations Valid up to 1,130°C and 2.2 GPa." *Contributions to Mineralogy and Petrology* 163, no. 5: 877–895. https://doi.org/10.1007/s00410-011-0704-6.

Shaw, H. R. 1972. "Viscosities of Magmatic Silicate Liquids; an Empirical Method of Prediction." *American Journal of Science* 272, no. 9: 870–893. https://doi.org/10.2475/ajs.272.9.870.

Shukuno, H., Y. Tamura, K. Tani, Q. Chang, T. Suzuki, and R. S. Fiske. 2006. "Origin of Silicic Magmas and the Compositional Gap at Sumisu Submarine Caldera, Izu-Bonin Arc, Japan." *Journal of Volcanology and Geothermal Research* 156, no. 3–4: 187–216. https://doi.org/10.1016/j.jvolgeores.2006.03.018.

Smith, I. E. M., and R. C. Price. 2006. "The Tonga-Kermadec Arc and Havre-Lau Back-Arc System: Their Role in the Development of Tectonic and Magmatic Models for the Western Pacific." *Journal of Volcanology and Geothermal Research* 156, no. 3–4: 315–331. https://doi.org/10.1016/j.jvolgeores.2006.03.006.

Smith, I. E. M., R. B. Stewart, and R. C. Price. 2003. "The Petrology of a Large Intra-Oceanic Silicic Eruption: The Sandy Bay Tephra, Kermadec Arc, Southwest Pacific." *Journal of Volcanology and Geothermal Research* 124, no. 3–4: 173–194. https://doi.org/10.1016/S0377-0273(03)00040-4.

Smith, I. E. M., R. B. Stewart, R. C. Price, and T. J. Worthington. 2010. "Are Arc-Type Rocks the Products of Magma Crystallisation? Observations From a Simple Oceanic Arc Volcano: Raoul Island, Kermadec Arc, SW Pacific." *Journal of Volcanology and Geothermal Research* 190, no. 1–2: 219–234. https://doi.org/10.1016/j.jvolgeores.2009.05.006.

Smith, I. E. M., T. J. Worthington, R. B. Stewart, R. C. Price, and J. A. Gamble. 2003. "Felsic Volcanism in the Kermadec Arc, SW Pacific: Crustal Recycling in an Oceanic Setting." *Geological Society, London, Special Publications* 219, no. 1: 99–118. https://doi.org/10.1144/GSL.SP.2003.219.01.05.

Spencer, K. J., and D. H. Lindsley. 1981. "A Solution Model for Coexisting Fe-Ti Oxides." *American Mineralogist* 66: 1189–1201.

Sugawara, T. 2000. "Empirical Relationships Between Temperature, Pressure, and MgO Content in Olivine and Pyroxene Saturated Liquid." *Journal of Geophysical Research: Solid Earth* 105, no. B4: 8457–8472. https://doi.org/10.1029/2000JB900010.

Tamura, Y., J. B. Gill, D. Tollstrup, et al. 2009. "Silicic Magmas in the Izu-Bonin Oceanic Arc and Implications for Crustal Evolution." *Journal of Petrology* 50, no. 4: 685–723. https://doi.org/10.1093/petrology/egp017.

Tamura, Y., O. Ishizuka, T. Sato, and A. R. L. Nichols. 2019. "Nishinoshima Volcano in the Ogasawara Arc: New Continent From the Ocean?" *Island Arc* 28, no. 1: 1–20. https://doi.org/10.1111/iar.12285.

Tamura, Y., O. Ishizuka, R. Stern, et al. 2014. "Mission Immiscible: Distinct Subduction Components Generatetwo Primary Magmas at Pagan Volcano, Mariana Arc." *Journal of Petrology* 55, no. 1: 63–101. https://doi.org/10.1093/petrology/egt061.

Tamura, Y., T. Sato, T. Fujiwara, S. Kodaira, and A. Nichols. 2016. "Advent of Continents: A New Hypothesis." *Scientific Reports* 6, no. 1: 33517. https://doi.org/10.1038/srep33517.

Tamura, Y., and Y. Tatsumi. 2002. "Remelting of an Andesitic Crust as a Possible Origin for Rhyolitic Magma in Oceanic Arcs: An Example From the Izu–Bonin Arc." *Journal of Petrology* 43, no. 6: 1029–1047. https://doi.org/10.1093/petrology/43.6.1029.

Tatsumi, Y., and T. Suzuki. 2009. "Tholeiitic vs Calc-alkalic Differentiation and Evolution of Arc Crust: Constraints from Melting Experiments on a Basalt from the Izu-Bonin-Mariana Arc." *Journal of Petrology* 50, no. 8: 1575–1603. https://doi.org/10.1093/petrology/egp044.

Taylor, R. N., R. W. Nesbitt, P. Vidal, R. S. Harmon, B. Auvray, and I. W. Croudace. 1994. "Mineralogy, Chemistry, and Genesis of the Boninite Series Volcanics, Chichijima, Bonin Islands, Japan." *Journal of Petrology* 35, no. 3: 577–617. https://doi.org/10.1093/petrology/35.3.577.

Tilhac, R., K. Hidas, B. Oliveira, and C. J. Garrido. 2023. "Evidence of Ghost Plagioclase Signature Induced by Kinetic Fractionation of Europium in the Earth's Mantle." *Nature Communications* 14, no. 1: 1099. https://doi.org/10.1038/s41467-023-36753-0.

Timm, C., B. Davy, K. Haase, et al. 2014. "Subduction of the Oceanic Hikurangi Plateau and Its Impact on the Kermadec Arc." *Nature Communications* 5: 4923. https://doi.org/10.1038/ncomms5923.

Timm, C., I. J. Graham, C. E. J. De Ronde, M. I. Leybourne, and J. Woodhead. 2012. "Geochemical Evolution of Monowai Volcanic Center: New Insights Into the Northern Kermadec Arc Subduction System, SW Pacific." *Geochemistry, Geophysics, Geosystems* 12, no. 8: 1–20. https://doi.org/10.1029/2011GC003654.

Timm, C., M. I. Leybourne, K. Hoernle, et al. 2016. "Trench-Perpendicular Geochemical Variation Between Two Adjacent Kermadec Arc Volcanoes Rumble II East and West: The Role of the Subducted Hikurangi Plateau in Element Recycling in Arc Magmas." *Journal of Petrology* 57, no. 7: 1335–1360. https://doi.org/10.1093/petrology/egw042.

Turner, S., C. Hawkesworth, N. Rogers, et al. 1997. "238U-230Th Disequilibria, Magma Petrogenesis, and Flux Rates Beneath the Depleted Tonga-Kermadec Island Arc." *Geochimica et Cosmochimica Acta* 61, no. 22: 4855–4884. https://doi.org/10.1016/S0016-7037(97)00281-0.

Umino, S. 1986. "Magma Mixing in Boninite Sequence of Chichijima, Bonin Islands." *Journal of Volcanology and Geothermal Research* 29, no. 1–4: 125–157. https://doi.org/10.1016/0377-0273(86)90042-9.

Velasquez, E., S. E. Bryan, M. Ekins, A. G. Cook, L. Hurrey, and J. Firn. 2018. "Age and Area Predict Patterns of Species Richness in Pumice Rafts Contingent on Oceanic Climatic Zone Encountered." *Ecology and Evolution* 8, no. 10: 5034–5046. https://doi.org/10.1002/ece3.3980.

Wang, X., T. Hou, M. Wang, et al. 2021. "A New Clinopyroxene Thermobarometer for Mafic to Intermediate Magmatic Systems." *European Journal of Mineralogy* 33, no. 5: 621–637. https://doi.org/10.5194/ejm-33-621-2021.

Waters, L. E., and R. A. Lange. 2015. "An Updated Calibration of the Plagioclase-Liquid Hygrometer-Thermometer Applicable to Basalts Through Rhyolites." *American Mineralogist* 100, no. 10: 2172–2184. https://doi.org/10.2138/am-2015-5232.

Wright, I. C., T. J. Worthington, and J. A. Gamble. 2006. "New Multibeam Mapping and Geochemistry of the 30°-35° S Sector, and Overview, of Southern Kermadec Arc Volcanism." *Journal of Volcanology and Geothermal Research* 149, no. 3–4: 263–296. https://doi.org/10.1016/j.jvolgeores.2005.03.021.

Wysoczanski, R. J., M. R. Handler, C. I. Schipper, et al. 2012. "The Tectonomagmatic Source of Ore Metals and Volatile Elements in the Southern Kermadec Arc." *Economic Geology* 107, no. 8: 1539–1556. https://doi.org/10.2113/econgeo.107.8.1539.

Yoshida, K., A. Miyake, S. H. Okumura, et al. 2023. "Oxidation-Induced Nanolite Crystallization Triggered the 2021 Eruption of Fukutoku-Oka-No-Ba, Japan." *Scientific Reports* 13, no. 1: 7117. https://doi.org/10.1038/s41598-023-34301-w.

Yoshida, K., Y. Tamura, T. Sato, et al. 2022. "Variety of the Drift Pumice Clasts From the 2021 Fukutoku-Oka-No-Ba Eruption, Japan." *Island Arc* 31, no. 1: e12441. https://doi.org/10.1111/iar.12441.

Supporting Information

Additional supporting information can be found online in the Supporting Information section. **Figure S1:** Petrographic characteristics of ankaramites. (a) Hand specimen of sample DR28-25. (b) Hand specimen of sample DR28-17. (c) Cross-polarized light photomicrograph of the whole thin section of sample DR28-25. Cpx, clinopyroxene; Ol, olivine; Vc, vesicle. The area outlined by the white rectangle is shown in (d). (d) Cross-polarized light photomicrograph of the groundmass. Pl = plagioclase. (e) Core–rim chemical compositions of phenocryst minerals. The diagonal line indicates a 1:1 relationship. Fo = 100 Mg/(Mg + Fe), Mg# = 100 Mg/(Mg + Fe), An = 100Ca/(Ca + Na + K). **Figure S2:** Petrographic characteristics of basalts. (a) Cross-polarized light photomicrograph of the whole thin section of sample DR29-1. The area outlined by the white rectangle is shown in (c). (b) Cross-polarized light photomicrograph of the whole thin section of sample DR22-1. The area outlined by the white rectangle is shown in (d). (c) Photomicrograph of sample DR29-1 showing an olivine + clinopyroxene + plagioclase glomerocryst. Cpx, clinopyroxene; Ol, olivine; Pl, plagioclase. (d) Photomicrograph of sample DR22-1. (e) Core–rim chemical compositions of phenocryst minerals. The diagonal line indicates a 1:1 relationship. Fo = 100 Mg/(Mg + Fe), Mg# = 100 Mg/(Mg + Fe), An = 100Ca/(Ca + Na + K). **Figure S3:** Petrographic characteristics of magnesian andesite from DR25. (a) Hand specimen of sample DR25-2 showing quenched glass on the surface. (b) Plane-polarized light photomicrograph of the whole thin section of sample DR25-2. The area outlined by the white rectangle is shown in (c), (d), and (e). (c) Photomicrograph showing olivine and clinopyroxene microphenocrysts. Cpx, clinopyroxene; Ol, olivine. (d) Clinopyroxene microphenocryst. (e) Back-scattered electron image of an olivine xenocryst, consisting of a forsteritic core (Fo92) mantled by a thin rim (Fo85) similar in composition to the microphenocrysts. (f) Stereomicroscope image of quenched glass containing minor acicular quench crystals. (g) Core–rim chemical compositions of phenocryst minerals. The diagonal line indicates a 1:1 relationship. Fo = 100 Mg/(Mg + Fe), Mg# = 100 Mg/(Mg + Fe). **Figure S4:** Petrographic characteristics of low-Mg andesites. (a) Cross-polarized light photomicrograph of the whole thin section of sample DR26-1. The area outlined by the white rectangle is shown in (c). (b) Cross-polarized light photomicrograph of the whole thin section of sample DR26-2. The area outlined by the white rectangle is shown in (d). (c) Photomicrograph of sample DR26-1. Cpx, clinopyroxene; Ilm, ilmenite; Opx, orthopyroxene; Pl, plagioclase. (d) Photomicrograph of sample DR26-2 showing a clinopyroxene + orthopyroxene + plagioclase glomerocryst. (e) Core–rim chemical compositions of phenocryst minerals. The diagonal line indicates a 1:1 relationship. Mg# = 100 Mg/(Mg + Fe), An = 100Ca/(Ca + Na + K). **Figure S5:** Petrographic characteristics of dacites. (a) Cross-polarized light photomicrograph of the whole thin section of sample DR27-5. The area outlined by the white rectangle is shown in (c). (b) Cross-polarized light photomicrograph of the whole thin section of sample DR27-9. The area outlined by the white rectangle is shown in (d). (c) Photomicrograph of sample DR27-5. Hbl, hornblende; Mgt, magnetite; Opx, orthopyroxene; Pl, plagioclase. (d) Photomicrograph of sample DR27-9 showing a clinopyroxene + orthopyroxene + plagioclase glomerocryst. Cpx, clinopyroxene. (e) Core–rim chemical compositions of phenocryst minerals. The diagonal line indicates a 1:1 relationship. Mg# = 100 Mg/(Mg + Fe), An = 100Ca/(Ca + Na + K). **Figure S6:** Petrographic characteristics of rhyolites. (a) Cross-polarized light photomicrograph of the whole thin section of sample DR27-1. The area outlined by the white rectangle is shown in (b). (b) Photomicrograph of sample DR27-1. Hbl, hornblende; Opx, orthopyroxene; Pl, plagioclase. (c) Core–rim chemical compositions of phenocryst minerals. The diagonal line indicates a 1:1 relationship. Mg# = 100 Mg/(Mg + Fe), An = 100Ca/(Ca + Na + K). **Figure S7:** The trace element ratios (Zr/Y, Nb/Yb) and Sr-Nd-Hf-Pb isotopic compositions do not change significantly during crystallization differentiations. Dacites and rhyolites are confined within the highlighted narrow limits, and the magnesian andesites are within the ranges These symbols are shown in Figure 1. The data were obtained from Hirai et al. (2023, 2024). **Figure S8:** SiO_2 versus remaining liquid fractions for the basalt and HMA differentiation models under variable pressure, water content, and oxygen fugacity conditions. Filled and open stars denote SiO_2 contents of PBMIs and Kibblewhite HMAs, respectively. **Table S1:** Summary of magma conditions estimated by geothermobarometers. **Table S2:** Results of least-squares fractional crystallization modeling. **Table S3:** Summary of mass balance fractional crystallization modeling for HMA and basalt differentiation models. **Table S4:** Initial melt compositions used in the thermodynamic modeling.